Natural Alkaloid Berberine Activity against Pseudomonas aeruginosa MexXY-Mediated Aminoglycoside Resistance: In Silico and in Vitro Studies

Natural alkaloid berberine activity against *Pseudomonas aeruginosa* MexXY-mediated aminoglycoside resistance: *in silico* and *in vitro* studies.

Emiliano Laudadio[1], Nicholas Cedraro[2], Gianmarco Mangiaterra[2], Barbara Citterio[3], Giovanna Mobbili[2], Cristina Minnelli[2], Davide Bizzaro[2], Francesca Biavasco*[2], Roberta Galeazzi[2]*

[1] Dipartimento S.I.M.A.U., Università Politecnica delle Marche, via Brecce Bianche, 60131, Ancona, Italy;
[2] Dipartimento di Scienze della Vita e dell'Ambiente, Università Politecnica delle Marche, via Brecce Bianche, 60131, Ancona, Italy
[3]Dipartimento di Scienze Biomolecolari, sez. di Biotecnologie, Università degli Studi di Urbino "Carlo Bo", 61029 Urbino, Italy

Corresponding authors: Prof. R. Galeazzi, r.galeazzi@univpm.it; Prof. F. Biavasco, f.biavasco@univpm.it

ABSTRACT

The multidrug efflux system MexXY-OprM, inside the resistance-nodulation-division (RND) family, is a major determinant of aminoglycoside resistance in *Pseudomonas aeruginosa*. In the fight aimed to identify potential efflux pumps inhibitors (EPIs) among natural compounds, the alkaloid berberine emerged as a putative inhibitor of MexXY-OprM. In this work, we elucidated its interaction with the extrusor protein MexY and assessed its synergistic activity with aminoglycosides. In particular, we built an *in silico* model for the MexY protein in its trimeric association using both AcrB (*E. coli*) and MexB (*P. aeruginosa*) as 3D templates. This model has been stabilized in the bacterial cytoplasmic membrane using a molecular dynamics approach and used for ensemble docking to obtain the binding site mapping. Then, through dynamic docking, we assessed its binding affinity and its synergism with aminoglycosides focusing on tobramycin, which is widely used in the treatment of pulmonary infections. *In vitro* assays validated the data obtained: the results showed a two-fold increase of the inhibitory activity and 2-4 log increase of the killing activity of the association berberine-tobramycin compared to those of tobramycin alone against 13/28 tested *P. aeruginosa* clinical isolates. From hemolytic assays, we preliminary assessed berberine low toxicity.

Keywords: comparative molecular modeling, molecular docking, berberine, efflux pumps inhibitors, *Pseudomonas aeruginosa,* synergy tests.

INTRODUCTION

The Resistance-Nodulation-Division (RND) family multidrug efflux system MexXY-OprM is a major determinant of aminoglycoside resistance in *Pseudomonas aeruginosa.* It is mainly involved in the so called "adaptive resistance" [1-3] and its expression seems to be induced by different factors, in particular oxidative stress [4], drug-ribosome interactions [5] and translation impairment[6]. Moreover, in *P. aeruginosa agrW2* mutant strains, mutations in the *ParRS* system have been described as responsible for the efflux pump over-expression [7]. In the last years, many authors have underlined the high incidence of Multidrug-Resistant (MDR) *P. aeruginosa* strains overexpressing the MexXY-OprM pump in Cystic Fibrosis (CF) pulmonary infections; more importantly, it has been demonstrated that the bacterial growing in biofilm, a typical feature of chronic infections, leads to multiple-mutant clones, which mostly result in the inactivation of *mexZ*, the repressor of MexXY-OprM [8-9], resulting in aminoglycoside -resistance[10-11].

MexXY-OprM is a tripartite efflux pump including a periplasmic membrane fusion protein (MexX), the inner-membrane (IM) drug/H^+ antiporter (MexY; the RND component) and the outer membrane (OM) channel (OprM)[12]. Crystal structures of other *P. aeruginosa* efflux pump proteins such as MexB, as well as the related AcrB of *Escherichia coli*, indicate that RND components exist as asymmetric homotrimers whose individual monomers adopt, in a concerted fashion, one of three conformations that represent different steps of the drug export process: access, binding, and extrusion (also known as loose, tight, and open, respectively)[13,14]. Among the different efflux pumps expressed in *P. aeruginosa* strains, the MexXY-OprM represents the main mechanism of extrusion of aminoglycosides and other toxic molecules.

Some studies, aimed to elucidate the molecular basis of aminoglycoside recognition and export by MexY, identified the putative substrate-binding RND component by site-direct mutagenesis[15-16]. Lau et al. mapped the mutated residues in a 3D model of MexY built using a *in silico* homology modeling protocol starting from *Escherichia coli* AcrB as a template; as the main result, they identified in MexY a proximal binding pocket connected to a periplasm-linked cleft, which seems to play a role in aminoglycoside recognition[15]. Besides, Ruggerone et al. reported the MexY structure modeled using both AcrB and MexB structures as templates and analyzed the nature of the putative binding sites in MexY and MexB deduced from those identified in AcrB; anyway, in this study, no information arise from the possibility of the existence of allosteric inhibition sites[16].

The natural alkaloids berberine and palmatine, extracts from plants such as *Hydrastis Canadensis, Berberis aristata* and many others, have been shown to enhance antibiotic activity against *P. aeruginosa* overexpressing both MexAB and MexXY efflux pumps [17] and berberine (**Figure1**) resulted the most effective [18-19].

In relation to the EPI activity described by Morita et al. (2016)[19], we planned to investigate its interaction with the membrane transporter MexY and to gain further insights into its activity in combination with tobramycin, an antibiotic extensively used in the treatment of pulmonary infections[19], against *P. aeruginosa*.

Starting from these considerations, we planned to investigate its mechanism of action and to validate its activity in combination with tobramycin, an antibiotic largely used in the treatment of pulmonary infections[20], against *P. aeruginosa*. In a previous work aimed to find new inhibitors of the MexAB-mediated RND resistance we have identified two natural compounds (Morelloflavone and 3,6-dyhdroxypregna-20-one) resulting synergic with ciprofloxacin by a combined *in silico* and *in vitro* approach [21]. In the present paper, the same approach was used to predict the berberine binding model

and its affinity for MexY. Since the full resolved structure of this protein is still unavailable we built on a high-resolution model of MexY in its trimeric association using AcrB and MexB structures as 3D templates. The obtained model was stabilized in the bacterial cytoplasmic membrane using atomistic molecular dynamics (MD) simulations and then used to evaluate berberine binding affinity after we had mapped MexY binding sites by ensemble docking of natural compounds ZINC database.

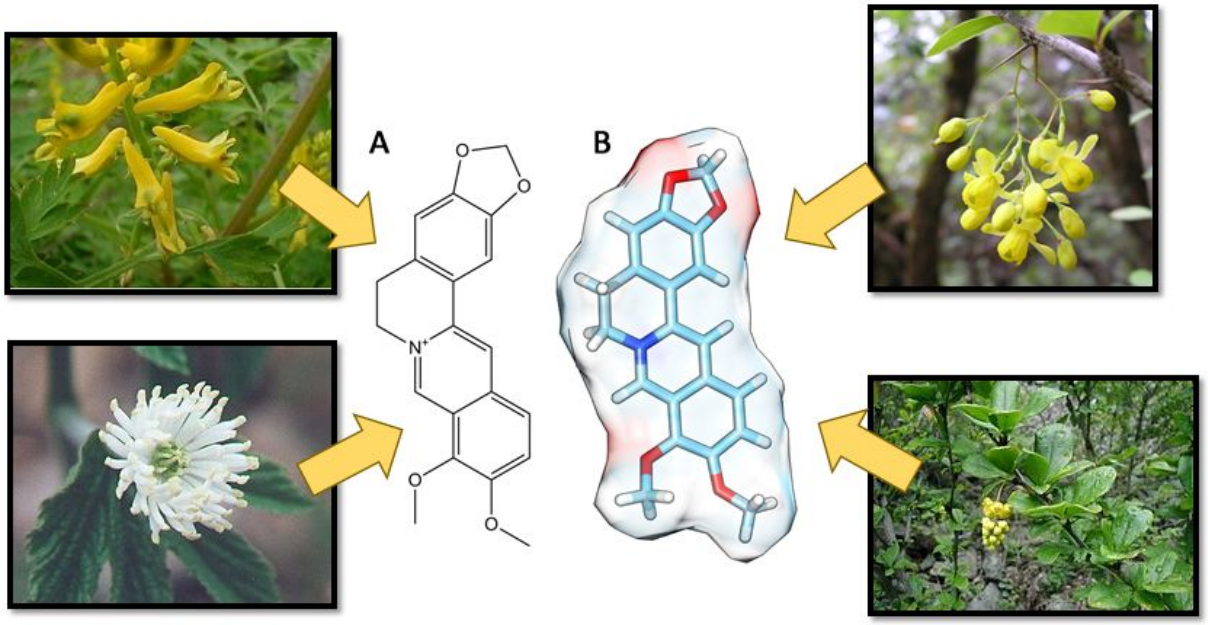

Figure 1. 2D (A) and 3D (B) berberine structure, alkaloid from *Coptis chinensis* (upper left), *Hydrastis canadensis* (down left), *Berberis aquifolium* (upper right), *Berberis vulgaris* (down right)

RESULTS AND DISCUSSION

MexY Comparative modeling and Site mapping

Starting from the X-ray crystal structures of AcrB (PDB code 1T9Y) and MexB (PDB code 2V50), we first built the monomeric model of MexY, followed by the corresponding trimeric complex, using a comparative modeling approach. The obtained model was energy minimized and then stabilized by full-atoms molecular dynamics simulation in its biological environment (i.e. bacterial membrane); the resulting structure was analyzed comparing its structural domains with those of the reference pump AcrB (**Figure 2**). As can be also observed for AcrB and MexB RND, monomers are formed by a transmembrane (TM) region of 12-helices (TM1-12), responsible for coupling the TM proton flux to pump operation, a periplasmic region divided into a IM-proximal porter domain of four strand/helix/strand subdomains (PC1, PC2, PN1, and PN2) involved in drug capture and extrusion, and an OM proximal region formed by two sheet subdomains (DN and DC) that form a so-called docking domain[13-15, 22-24]. For AcrB, two routes of drug access into the binding pockets have been described, one *via* a cleft between PC1 and PC2 (the cleft pathway)[25-26] and the other involving the inter-monomers vestibule found near the IM surface and, possibly, a hydrophobic groove defined by TM8 and TM9 (the vestibule pathway) [26]. Evidence suggests that the cleft route is used by larger and, likely, hydrophilic substrates whereas the vestibule pathway accommodates lipophilic agents that are likely to partition into the IM [26].

In order to identify the most probable ligand-binding sites for MexY, ensemble docking using ZINC natural compounds databases was performed against the built model of MexY (see *Supplementary information* for more details). Efflux pumps binding clefts were mapped based on the ligands' predicted binding energy and the corresponding cluster population. More in details, all the compounds of the database (see Material and Methods) were blind docked to MexY using Autodock Vina, considering the grid potential spread all over the protein surface; the resulting docked poses were clustered according to the protein regions in which the ligands bind and finally the resulting clusters were ranked on the basis of the predicted binding energy and their population. Only cluster including a number of compounds > 10 were considered.

As a result, we confirmed for MexY the existence of the same two polyspecific binding pockets with high affinity already identified in AcrB and MexB, namely site 1 and site 2 (**Figure 3**) corresponding to the external periplasmic accession site and to the extrusion antibiotic site respectively (**Table 1, Figure 3**); these two sites are accessible both in the tight monomer and in its trimeric form (**Figure 3**). In addition, we identified other two allosteric poses, one located to the inner transmembrane α-helices (site 4) and another located at the oligomerization surface that was thus discarded (site 3) (**Table 1, Figure 3**).

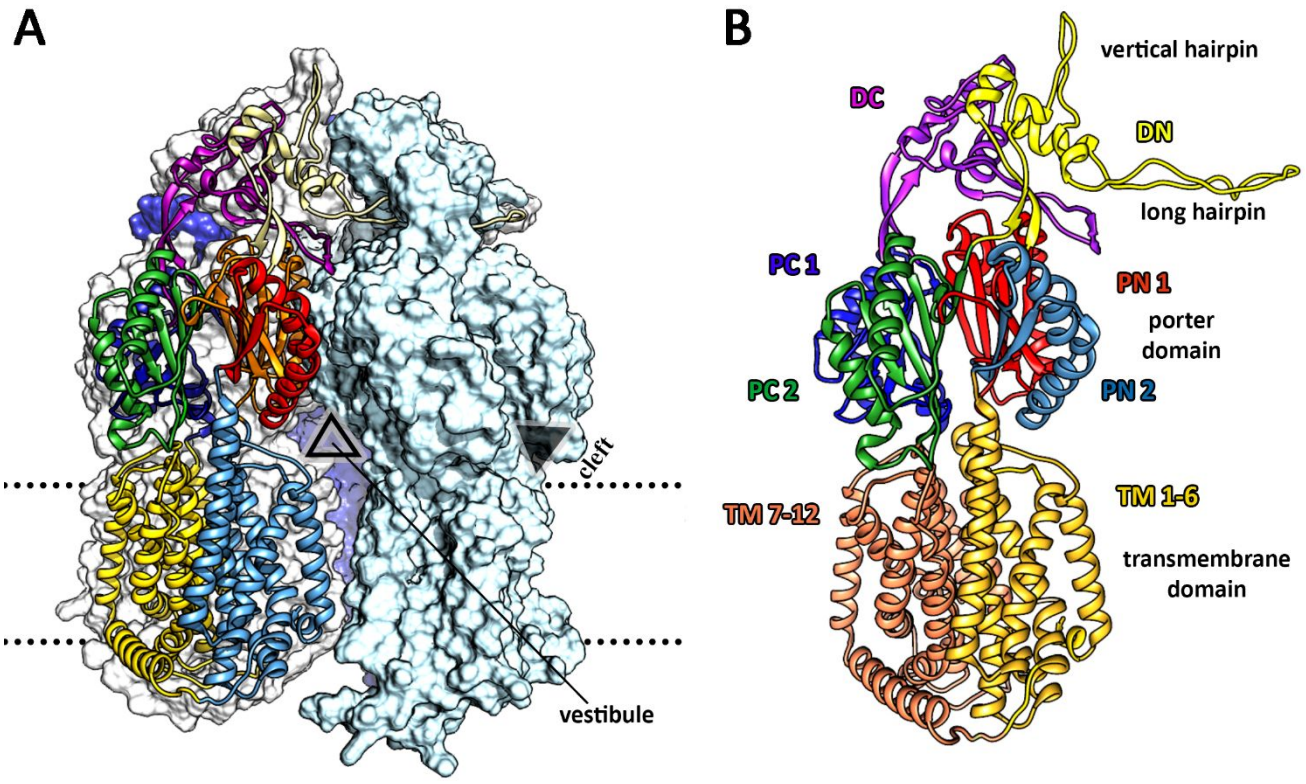

Figure 2. Trimeric (A) and monomeric (B) association of MexY protein. Main structural features of MexY as determined by comparison with the homologous membrane transporter AcrB [25]

Table 1. Amino-acidic compositions of MexY binding sites 1-4

Site		Residues
Site 1	cleft	Asp565, Gln566, Gly567, Gly640, Arg645, Glu648, Arg649, Leu666, Pro667, Arg678, Ala713, Gly714, Leu829, Gln830, Gln831, Arg832, Glu833, Ala834, Met835, Asn918, Asp919, Ile920, Tyr921, Thr999
Site 2	antibiotic site	Val42, Asn44, Ser46, Lys79, Ala80, Thr81, Leu89, Thr90, Leu91, Ala132, Asp133, Ser134, Ile135, Gln136, Val174, Gln575, Asp615, Gly616, Thr617, Ser618, Ser619, Asp676, Ala718, Gln814, Leu816, Leu818, Gly825, Ala827

Site 3	interface	Pro31, Pro36, Asp37, Ile38, Ala39, Pro40, Pro41, Gly96, Val97, Asn98, Asn100, Gly295, Ser296, Gly386, Phe387, Ser388, Ile389, Val391, Pro454, Phe457, Phe458, Val462, Ile465, Gln468, Phe469, Thr472, Val475
Site 4	membrane	Leu520, Arg523, Tyr524, Asn526, Ala527, Gly530, Ala533, Arg534, Val541, Leu544, Val545, Gly547, Val548, Val970, Leu974

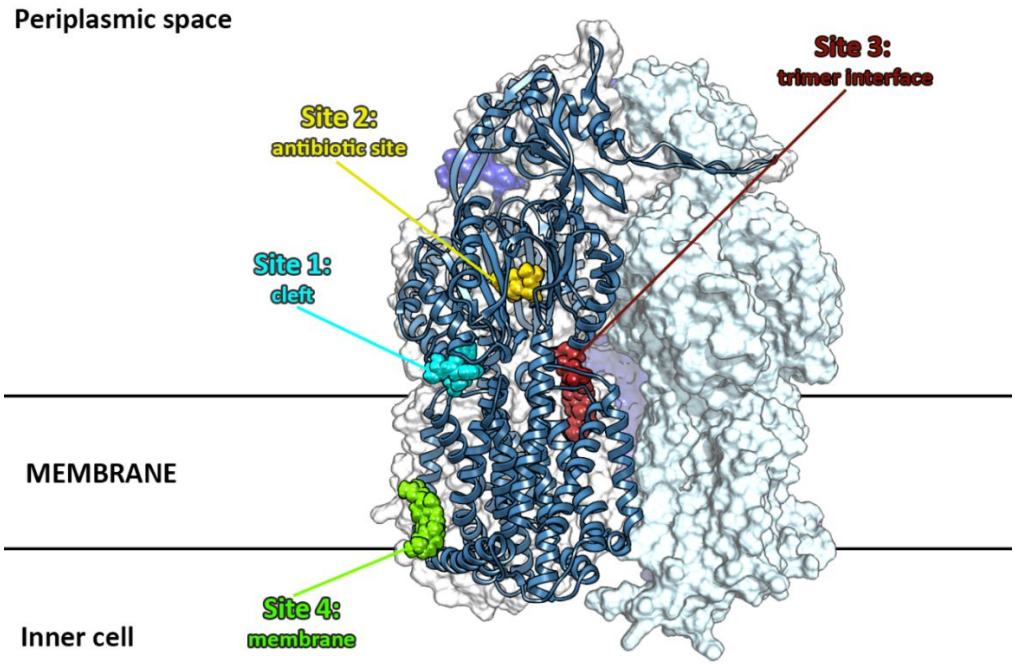

Figure 3. Localization of sites 1-4 onto the monomeric MexY protein from ensemble docking (S.I). The figure shows the trimer surface to better visualize the dispositions of the four found binding sites. In each site, we represent a bounded representative structure of the tested compounds (CPK models).

More in details, we found out that the highest active compounds, showing a binding energy lower than -10.0 kcal/mol (corresponding to nanomolar activity), bind exclusively to site 1 and 2. Compounds binding tightly only to site 3, show a lower protein binding affinity and in addition, due to its intermembrane location, they will hardly reach efficiently the target protein. For this structural feature, site 3 cannot contribute to the action mechanism and thus it has been excluded.

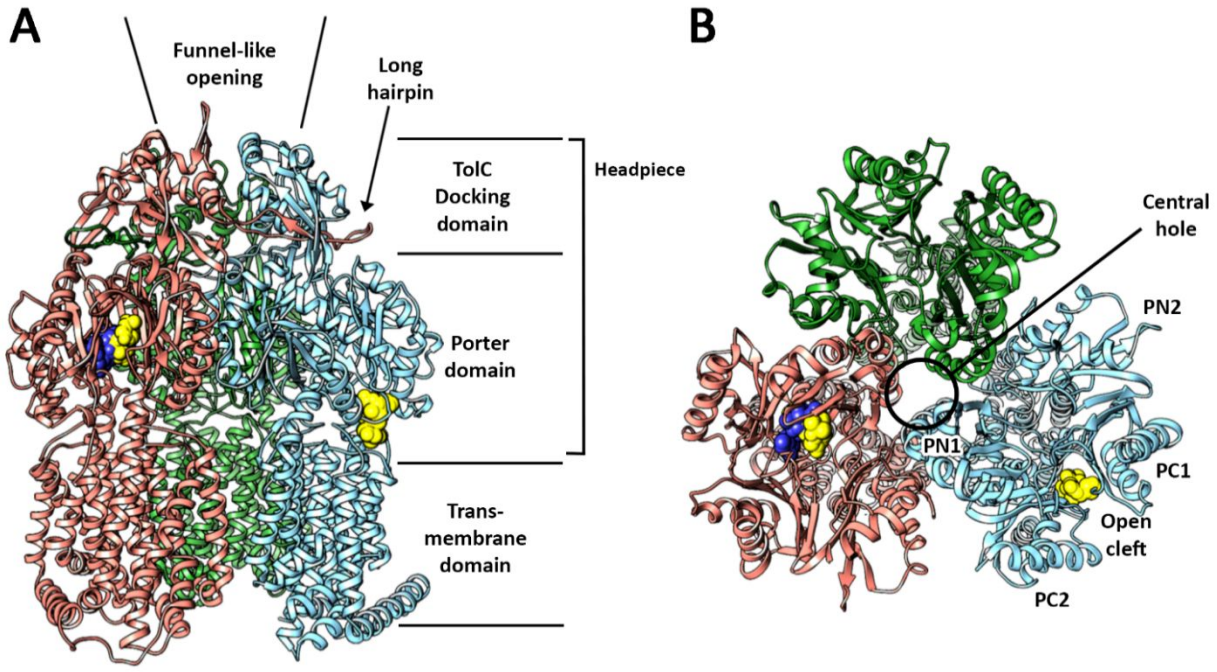

Figure 4. Front view (A) and top view (B) of MexY in its trimeric form. We report the three monomers in orange, green and light blue. The yellow spheres represent a "hit compound" put in each of the two possible binding sites (site 1-2), while the blue spheres represent tobramycin in its docked pose (site 2).

Berberine docking and dynamics with MexY in membrane

We proceeded to evaluate berberine's affinity for the extrusion protein MexY and its eventual competitiveness with the tobramycin uptake; for this purpose, blind docking of both berberine and the aminoglycoside has been performed and for each compound we observed only one populated binding cluster, corresponding to site 2 (the putative antibiotic extrusion site) (**Figure 4-5**). None of the identified poses corresponded to the allosteric external site (site 1) found out for inhibitors of other efflux pumps i.e. MexB, AcrB [21, 27]. Following our tested protocol[28-32], we re-docked the two compounds in site 2 for better positioning inside it (Focused docking) and the best docked pose for each compound (berberine and tobramycin) was then used as starting structure to carry out MD stabilization and MM-PBSA free energy calculation.

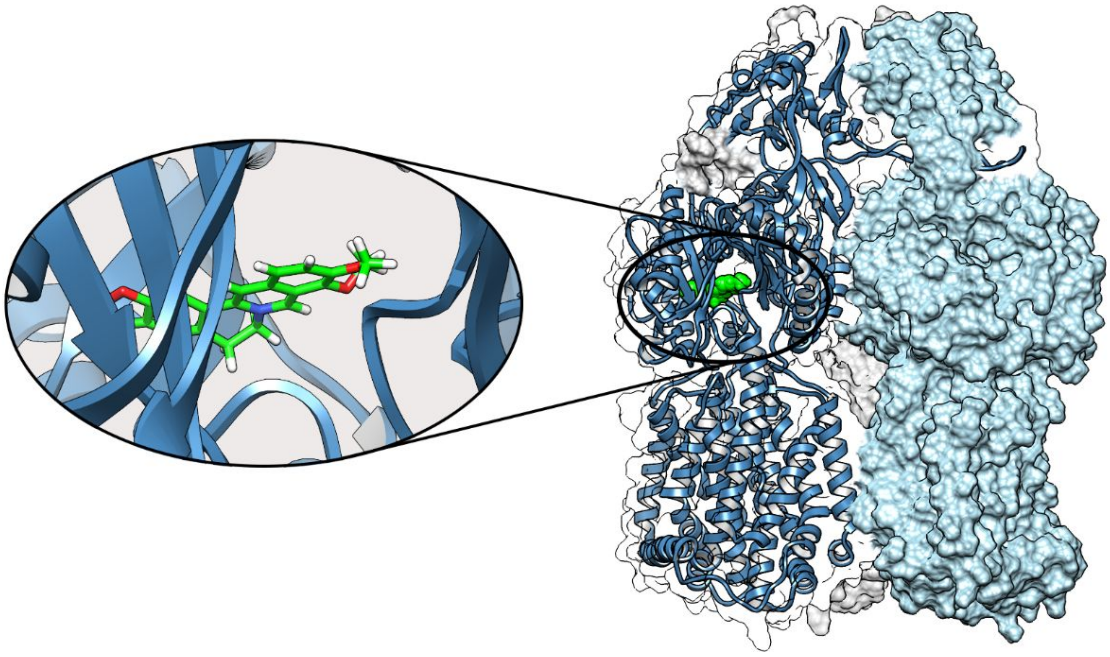

Figure 5. Berberine (represented in green) in binding site 2 of MexY trimer (represented in blue ribbon and white and light blue surfaces)

The ligand-bound MexY monomeric receptor has been rebuilt in its trimeric structural form and inserted into a lipid bilayers matrix, mimicking the periplasmic membrane. Then, in this trimeric structure, the dynamical stabilization of the two ligand-MexY complexes were carried out, namely MexY complexed only with either tobramycin (Model 1) or berberine docked in site 2 (Model 2), the only assessed cleft for both the alkaloid and the antibiotic (see previous section). Tobramycin and berberine compete for the same site and thus they cannot be considered at the same time.

The two models underwent a complete minimization protocol prior to proceed with MD simulations within the GROMACS software package framework[33] (*Experimental Section*). After dynamical stabilization of the ligands inside their binding sites (see *Supplementary Information*), we carried out MM-PBSA analysis to calculate the complexes' free energies. MexY-berberine complex showed a much lower free energy with respect the MexY-tobramycin one (**Table 2**); this means that the alkaloid has higher binding affinity than antibiotic for site 2 and we expect it can act as competitor of the antibiotic, preventing its extrusion. Concerning the estimated free energy (*Supplementary Information, **Figure S2***), during MD we observed an increase of total energy in MexY-tobramycin model, starting from a value of -684.56 ± 9.6 KJ/mol to -402.43± 9.7 KJ/mol at the end of the simulation. This behavior is probably due to the natural undergoing process of tobramycin extrusion, which is not observed in model with berberine since the free energy of binding remains quite the same (**Figure S2**), suggesting a high stability of the complex berberine-MexY, which is a basis for an efficient competitive mechanism that can prevent the antibiotic extrusion.

Table 2. Average free Gibbs energy for the docked complexes calculated on the last 2 ns of MD Simulations.

MexY transporter with	Free Energy ΔG_{bind} (KJ/mol)
berberine (site 2)	-864.31 ± 80.79
tobramycin (site 2)	-454.02 ± 75.44

In order to shed light on tobramycin-MexY interaction, we analyzed the complex structure, both at the beginning and during MD stabilization. Observing it at the equilibration step (starting structure), we found that tobramycin makes several H Bonds (up to nine, involving Lys79, Leu89, Leu91, Ser134, Phe677, two with Asp681, Tyr816, Ala825), but in the stabilized state, the number of H-bonds reduces (from nine to six involving Ser134, two with Asp676, two with Tyr816, Ala825) and it totally changes its positioning in the binding cleft. This feature correlates also with the calculated decrease of the free energy that determines the antibiotic extrusion (**Figure 6**).

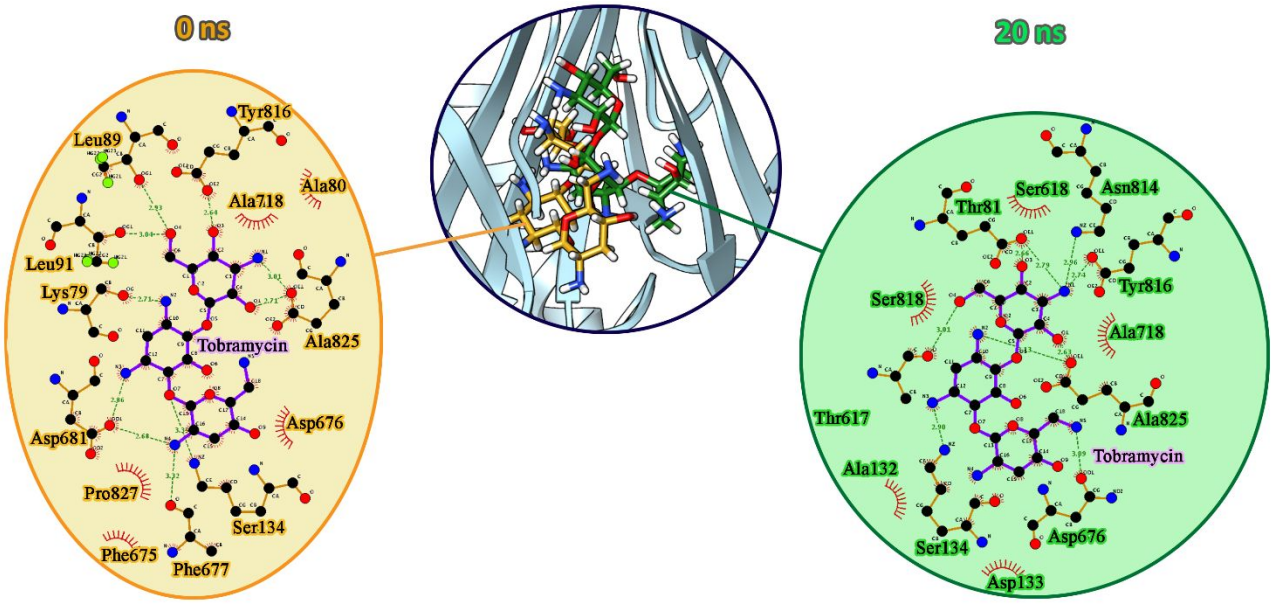

Figure 6. Stabilization of tobramycin (starting structure in yellow, ending structure in green) in site 2, in tobramycin-MexY model. We report the 2D environment around the antibiotic.

Besides, we also analyzed berberine's interactions with the cleft residues along MD stabilization trajectory. We found out that the alkaloid does not make any H-bonds but it is strongly stabilized by hydrophobic/stacking interactions, involving in particular Trp177, Phe610, Tyr613 (**Figure 7**) and Phe675, Phe677. The hydrophobic effect is a major driving force in biology, and it is a consequence of the geometries of the molecules and the detailed balance of the different energy terms. The residue Asp676 is instead involved in fixing the polar methoxyl groups in the binding site. These mentioned interactions were retained through all the MD simulation duration and keep berberine almost in its original orientation; this is due primary to the high hydrophobic energetic contribution and it corresponds to a small variation of the free Gibbs energy between the stating and the stabilized complex structure (Figure S2, SI).

Thus, we observed a very different behavior between the alkaloid inhibitor and the antibiotic: the latter undergoes major repositioning inside the cleft while the former only stabilizes/adjusts its binding pose. Indeed, the adjustment of the ligand pose inside its binding cleft is quite common in those cases in which the cleft is much larger than the ligands' volume, as is the case of site 2. This adjustment can thus also be associated to the variation of the aminoacids involved in the specific interaction [21, 34-37]. In MexY, close to site 2 (also reported as DP site)[16] there is an enlargement of the cavity (AP site by Ruggerone et al 2018)[16] considerably larger in MexB and MexY than in AcrB, where it is known as proximal multisite drug-binding pocket; [16, 36,37] this suggests the possibility for a ligand to bind in different orientations and/or at different sub-pockets, a hypothesis compatible with the multisite-drug-oscillation [36] and diffuse binding [37] in these proteins.

A criterion to be sure of the complete repositioning consists in the minimization of the binding energy and the preachment of a stationary state in which the interaction with specific residues are no more variated, even if we proceed to further extension of the MD trajectory.
Indeed, the tobramycin major changes in amino-acid interactions is also associated to energetic variation (see figure S2 reported in Supplementary Information) that can be ascribed to the slow extrusion motion that the antibiotic undergoes from this protein cleft; thus it cannot converge to a real stationary state since it moves upside along the protein central hole; extending the simulation, we expect to observe a further moving along the membrane long axis Z.

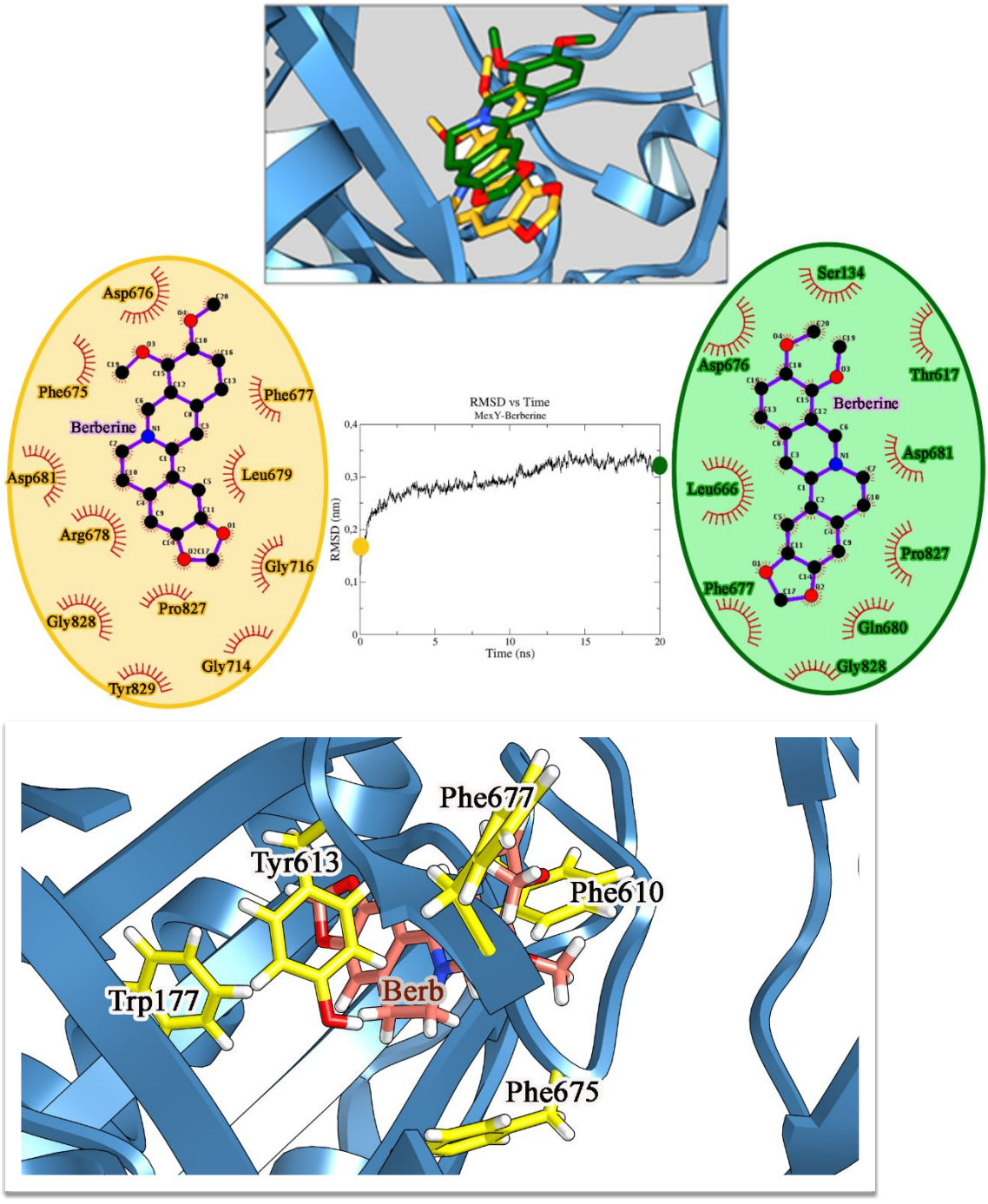

Figure 7. *Upper*. Figure 7. Stabilization of berberine starting (yellow) and ending (green) structures in site 2. We report the 2D environment around the antibiotic compound by Ligplot representation (only residues

present in the projection plane are visible). *Down*. 3D view of the main hydrophobic/staking interactions for berberine in the stabilized final state

Tobramycin susceptibility assays

Tobramycin minimal inhibitory concentration and resistance genes. Thirty *P. aeruginosa* strains (i.e. 28 clinical isolates and the reference strains *P. aeruginosa* PA14 and *P. aeruginosa* K767) were analyzed for their susceptibility to tobramycin by MIC determination and for the presence of the constitutive (*mexY* and *ndvB,*) and acquired (*rmtA* and *ant(2")-Ia*) tobramycin resistance genes by PCR assays.

Twenty-two exhibited MICs ranging from 8 to >128 µg/ml (**Table 3**); as expected *mexY* and *ndvB* were detected in all tested isolates, *rmtA* was never found, and *ant(2")-Ia* was found in only one strain (i.e. C89). Considering that *ndvB* has been described as a major *P. aeruginosa* resistance determinant when growing in biofilm and poorly expressed in planktonic conditions[38] and that the tobramycin MIC was determined using planktonic cells, we can consider the efflux pump MexXY-OprM as the main responsible for tobramycin resistance [2].

Checkerboard assays

To test the synergistic effect of berberine in combination with tobramycin, we performed checkerboard assays using doubling concentrations of both compounds (tobramycin from 0.125 to 128 µg/ml and berberine from 10 to 320 µg/ml) and the strain *P. aeruginosa* C25, a CF isolate selected due to *mexY* overexpression (five-fold compared to *P. aeruginosa* PAO1) and the lack of acquired tobramycin resistance genes.

Berberine showed no antibacterial activity up to 320 µg/ml. A significant reduction (16-fold, from 16 to 1 µg/ml) of the tobramycin MIC was observed when used in combination with berberine at concentrations ranging from 80 to 320 µg/ml. The synergistic activity of the association tobramycin-berberine was confirmed by the results obtained with 12 additional *P. aeruginosa* clinical isolates (**Table 3**). This supports the MexY-berberine docking results in showing the EPI activity of this alkaloid.

The lack of synergy observed in 17 *P. aeruginosa* strains is currently under investigation, considering the presence of mutations in the *mexY* gene. By contrast with MexB, the aminoacid sequence of MexY is indeed quite variable among the different *P. aeruginosa* isolates. This suggests the possible presence of important aminoacid modifications in the sequence of MexY which can affect the MexY 3D-structure and its binding with berberine. Experiments are in progress to investigate the presence of such mutations in the strains for which the susceptibility to tobramycin resulted unaffected by the association with berberine. Suitable changes in the natural compound structure (i.e. able to interfere with the structural changes detected in the MexY) will be then carried out to improve its binding affinity and the resulting EPI activity will be evaluated by *in vitro* microbiological tests.

Table 3. Tobramycin MIC in absence/presence of 80 µg/ml berberine against the 30 *P. aeruginosa* isolates. Tobramycin breakpoints: S≤4 µg/ml, I=8 µg/ml, R≥16 µg/ml [34].

STRAIN	MIC (µg/ml)	
	TOBRAMYCIN	TOBRAMYCIN AND BERBERINE
P. aeruginosa PA14 (N)	0,125	0,125
P. aeruginosa K767 (N)	0,25	0,125
P. aeruginosa C6 (N)	2	0,5*
P. aeruginosa C9 (M)	2	1
P. aeruginosa C15 (N)	8	8

P. aeruginosa C25 (M)	16	1*
P. aeruginosa C30 (N)	8	8
P. aeruginosa C31 (N)	8	8
P. aeruginosa C51 (N)	0,125	<0,125
P. aeruginosa C52 (N)	>128	128
P. aeruginosa C54 (N)	32	16
P. aeruginosa C59 (N)	64	32
P. aeruginosa C60 (N)	>128	64*
P. aeruginosa C61 (N)	64	16*
P. aeruginosa C67 (N)	16	16
P. aeruginosa C70 (N)	32	8*
P. aeruginosa C73 (N)	128	64
P. aeruginosa C76 (N)	32	16
P. aeruginosa C83 (M)	128	32*
P. aeruginosa C84 (N)	0,5	0,125*
P. aeruginosa C86 (N)	128	16*
P. aeruginosa C89 (N)	>128	64*
P. aeruginosa C93 (N)	>128	64*
P. aeruginosa C95 (N)	32	4*
P. aeruginosa C98 (N)	64	32
P. aeruginosa C103 (M)	4	4
P. aeruginosa C104 (N)	32	8*
P. aeruginosa AR48 (N)	32	8*
P. aeruginosa AR51 (N)	16	8
P. aeruginosa AR61 (M)	0,125	0,125

* reduction of tobramycin MIC ≥ 2fold
M, mucoid; N, non-mucoid

Killing curves

To compare the dynamic of the bactericidal activity of the different associations of tobramycin (1/2x, 1x, 2xMIC) and berberine (80 µg/ml), we performed killing curves assays against *P. aeruginosa* C95. This strain was selected since it showed a tobramycin MIC reduction comparable to that exhibited by *P. aeruginosa* C25, but faster growth in broth and a non-mucoid phenotype. When testing tobramycin alone, a reduction (2log) in the bacterial amount was only observed for concentrations corresponding to two-fold the MIC after 4, 6 and 8 h from antibiotic exposure. All tested antibiotic concentrations exhibited an increase of the *P. aeruginosa* surviving cells between 8 and 24 h, particularly evident for the 2xMIC. When used in association with berberine, tobramycin concentrations corresponding to 1xMIC and 2xMIC resulted bactericidal after 2 h and 1/2xMIC after 4 h from the exposure to the antibiotic. Moreover, when *P. aeruginosa* C95 was exposed to the MIC and 2xMIC of tobramycin in the presence of berberine, the 2log CFU reduction was maintained up to 24 h (**Figure 8**).

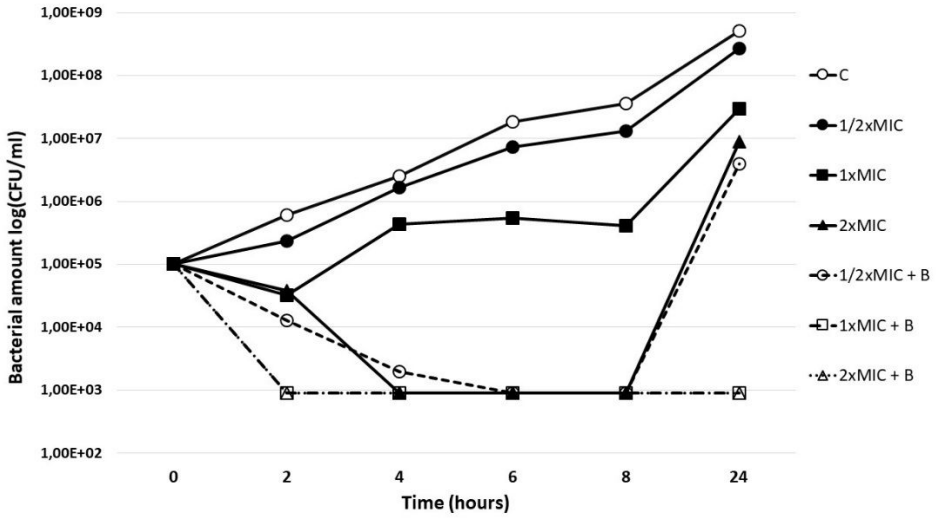

Figure 8. Time killing curve of *P. aeruginosa* C95 performed using no antibiotic (C) or 16 (1/2xMIC), 32 (MIC) and 64 µg/ml (2xMIC) of tobramycin, alone or in combination with 80 µg/ml Berberine (B)

Hemolytic activity determination

To evaluate the toxicity of berberine against human cell[40], we performed hemolytic assays using human red cells and the same berberine concentrations used in the checkerboard assays (i.e. from 10 to 320 µg/ml). None of the tested condition (neither the different berberine concentrations nor the solvent vehicle used as control) exhibited hemolytic activity thus enhancing the potential use of the berberine as EPI agent in the treatment of MDR P. aeruginosa infections.

CONCLUSIONS

Considering the alarming and increasing incidence of antibiotic resistance in *P. aeruginosa*, a combination therapy based on the association of an antibiotic and an active phytochemical seems a promising approach to counteract MDR *P. aeruginosa* infections. The ability to contrast the efflux-mediated resistance is important due to the involvement of different classes of antibiotics. As similarly reported for the MexAB-OprM inhibitors morelloflavone and pregna-20-one derivative against ciprofloxacin [21], in the present work the *in silico* protocol succeeded in justifying the putative ability of the alkaloid berberine to counteract the activity of the aminoglycoside extruder pump MexXY-OprM. Berberine and the aminoglycoside tobramycin resulted to be competitive for the extrusion site. The high difference in their relative free binding energy (**Table 2**) gives strong evidence for a possible inhibitory activity of the alkaloid against RDN resistance involving this efflux pump (MexY).

The *in silico* findings have been supported by drug combination assays, which showed the synergistic activity of the association berberine/tobramycin, against different clinical isolates of *P. aeruginosa,* demonstrated by the increase of both the inhibitory (up to 4-fold) and the killing (2 log decrease of the survival cells) activity of the association compared to those of the antibiotic alone. These data coupled with its lack of hemolytic activity warrant further studies aimed at the validation of berberine for the treatment of MDR *P. aeruginosa* infections.

EXPERIMENTAL SECTION

COMPUTATIONAL METHODS

Protein modeling. The 3D MexY model was built using the SWISSMODEL and I-TASSER server[41-43]. In particular, we focused our attention on a multiple template alignment strategy concerning the X-ray data of the available AcrB and MexB proteins. The amino acid sequence of full length MexY transporter P. aeruginosa PAO1 was retrieved from the SWISSPROT database[43] and from the UniProt database (The UniProt Consortium, 2015) (UNIPROT ID: Q9ZNG8),while the three-dimensional structure coordinates were obtained from the *E. coli* AcrB trimer and monomer (PDB accession number 2HRT and 1T9Y respectively) and the MexB monomers (PDB accession code 2V50) available from the Brookhaven Protein Data Bank (www.rcsb.pdb.org).

In total, two MexY models were generated with different geometric conformations but showing good least root mean square deviation (RMSD) with respect to trace (Cα atoms) of the template crystal structures. Further, refinement was performed in order to choose the best structure conformation resulting from SWISSMODEL. Besides, for further validation, the 3D models of MexY were also constructed using the I-TASSER server implemented in the multiple templates/threading protocol (http://zhanglab.ccmb.med.umich.edu/I-TASSER/).

The I-TASSER server is an online platform for protein structure and function predictions; the output of the I-TASSER server for each query includes up to five full-length models, the confidence score (C-score), the estimated TM-score and RMSD, and the standard deviation of the estimations. To select the final models, I-TASSER uses the SPICKER program to cluster all the decoys based on the pair-wise structure similarity, and reports up to five models, which corresponds to the five largest structure clusters. All the obtained models were then further refined according to the protocol reported in next section in order to choose the best 3D structure of the receptor.

Protein structure refinement and energy minimization. Structure refinement of the modeled MexY was performed using the KoBaMIN[44] web server (a knowledge-based minimization web server for protein structure refinement) in order to obtain the best conformation of modeled structures resulting from SWISSMODEL and I-TASSER sever. The KoBaMIN web server provides an online interface to a simple, consistent and computationally efficient protein structure refinement protocol based on minimization of a knowledge-based potential of mean force. Finally, the selected model underwent a full energy minimization protocol using AMBER94 force field within GROMACS 5.0 suite of programs[33]. The energy minimization was carried out by the 2000 steps of steepest descent followed by 2000 steps of conjugate gradient minimization until the RMS gradient of the potential energy was less than 0.1 kcal mol^{-1} $Å^{-1}$.

The stereochemical quality of the protein structure was checked by Ramachandran plot using the PROCHECK program[45].

Natural compound database for ensamble docking. Information on natural compounds with known antimicrobial and anticancer bioactivity was obtained from ZINC and associated Database (www.zinc.org); our plan was to start from pure natural origin compounds to better find out hits with different structure and to this purpose, we firstly screened the SPECnet ZINC database, integrated by an *in house* developed database (total number of tested compounds 2100). All their structures were retrieved from Pubchem database (pubchem.ncbi.nlm.nih.gov) and used as starting point for ligand preparation. Compounds were minimized by AMBER force field to reach the convergence of 0.05 Å. Charges were previously obtained using AM1-BCC Hamiltonian[46].

MexY Protein preparation for binding sites mapping by ensemble docking. The modeled protein was prepared for further investigation using CHIMERA[46]. Protein ionization was settled out considering a pH of 7.4, which corresponds to that of the experimental conditions, and the following physical parameters: salinity 0.15 M, internal dielectric 6, external dielectric 80[28-30, 47-50].

A Site map prediction for MexY protein was then accomplished using AcrB/MexB binding cavity as starting point and the subsequent virtual screening was carried out extending the grid calculations to the surrounding regions, in order to better evaluate other hidden putative bonding regions.

Ensemble docking *via* High throughput virtual screening (HTVS) of phytochemicals against MexY integral membrane protein. All screening molecular docking experiments were performed by AutoDock Vina version 1.1.2 [51] that has been demonstrated to be a high reliable VS software. [52-54] Then, the virtual screening software Vina was used to screen the collections of natural compounds against all the surface of MexY in order to identify putative binding sites.
Thus, at a first instance we extended the grid to cover all the protein surface (two different grid maps generations, each of 120X120x120 $Å^3$ centered on two different point). After the identification of the best scored poses, Autodock 4.2.1 (AD4) was used to refine the binding pose and relative energy [52,55]. The number of AD4 GA runs was increased up to 200 and the grid spacing kept at 0.375. Then, each identified site from this blind docking procedure has been refined in a focused docking strategy aimed to refine the docking poses and relative energies. The box of size 40X40X40 $Å^3$ has then been used centered onto the center of each identified bonding site. All the PDB structures were converted to PDBQT and then over 5000 structures from ZINC natural compounds databases were docked in the identified binding sites of the MexY receptor using the standard parameters of AutoDock Vina. The virtual screening workflow offers selective filtration of ligands with increased strictness on the bases of their efficiency to interact with the binding cavity residues (docking score function and binding energy). Before performing the docking, computational protocol was validated by evaluating the reproducibility of re-docking the co-crystallized ligand-receptor (RMSD 0.910 Å) complex (1T9Y), already tested by our group [23]. All the 100 independent GA runs from AD4 were processed using the built-in clustering analysis with a 2.0 Å cutoff (cluster analysis). The same blind docking/focused docking protocol was used for berberine and tobramycin.

Molecular dynamics of the MexY-ligand complexes in membrane. The MexY-inhibitor models have been oriented in membrane through OPM (Orientation of Proteins in Membrane) server (http://opm.phar.umich.edu/server.php), which generates the coordinates along the Z axis, and we used CHARMM GUI (www.charmm-gui.org) to build a membrane composed by 800 1-palmitoyl-2-oleoyl-*sn*-glycero-3-phosphocholine (POPC) molecules. Using these coordinates, we got a MexY-trimer (with docked ligands) system properly surrounded by the lipid matrix, that has been appropriately solvated with water (about 10000) and ions (to reach up 0.15M NaCl, adding 397 Na ions and 361 Cl ions also to balance the trimer charge). We used AMBER99SB-ILDN force field parameters[56] for the protein and lipids, the TIP3P [57] model for solvent as implemented in GROMACS 5 [33]. The models were minimized, and after then, six equilibration phases and molecular dynamics simulations were carried out. The overall time of simulation was 20 ns, time necessary for ligand stabilization inside the binding cleft. Indeed, 10-20 ns is the average time needed for the ligand to reorient itself inside the pocket prior its dynamical evolution [58-60]. In fact, as it results from RMSD graphs (see *Supplementary Information*), all the ligand-protein complexes reach a steady state (average deviation $\Delta RMSD=0.37\pm0.02$) starting from an initial different orientation thus supporting that 10-20 ns is a reasonable time in this case. The time-step used was 0.002 ps, and coordinates were written out every 10 ps, while energy data were collected every 2 ps. Periodic boundary conditions were applied in all directions using a neighbor searching grid type, and also setting at 1.4 nm the cut-off distance for the short-range neighbor list. Electrostatic were taken into account implementing a fast smooth Particle-Mesh Ewald algorithm (SPME), with a 1.4 nm distance for the Coulomb cut-off [61].
Free Gibbs Binding energy was calculated with the MM-PBSA method (Molecular Mechanics/Poisson Boltzmann Surface Area) using g_mmpbsa tool [62] with default settings. All 20 ns of production run in

the simulations were used and snapshots were extracted every 10 ps and energetic terms calculated. Results are in terms of average and standard deviations for all energetic components [63].

IN VITRO ASSAYS

Bacterial strains, growth media and antibiotics. Twenty-eight aminoglycoside-resistant clinical *P. aeruginosa* strains (10 from CF and 18 from non CF patients) were collected from the Microbiology labs of "Ospedali Riuniti" (Ancona, Italy) and "Ospedale A. Murri" (Fermo, Italy). *P. aeruginosa* PAO1 and PA14 [64-65] were kindly provided by professor Olivier Jousson (Integrated Biology Center, University of Trento, Trento, Italy), *P. aeruginosa* K767 (PAO1) was kindly provided by professor Keith Poole (Department of Biomedical and Molecular Sciences, Queen's university, Kingston, Canada). *P. aeruginosa* ATCC 27853 and *P. aeruginosa* AR86 belong to the strain collection of the Microbiology section of the Department of Life and Environmental Sciences (DiSVA) of the Polytechnic University of Marche (Ancona, Italy). All strains were cultured in Luria Bertani (LB) broth or agar, subcultured in McConkey (MC) agar and stocked at -80°C in LB broth supplemented with 20% glycerol.

Bacteriological media were purchased from Oxoid (Oxoid spa, Milano, Italy) and tobramycin from Sigma (Sigma Aldrich SRL, Milano, IT).

Antibiotic susceptibility tests.

The Minimal Inhibitory Concentration (MIC) of tobramycin was determined by the broth microdilution method in 96 wells-microtiter plates, following the CLSI guidelines [66], using *P. aeruginosa* ATCC 27853 as the reference strain. The results were evaluated after 24 and 48 h at 37°C to allow a visible growth of all tested strains.

Checkerboard assays and killing curves were performed as previously described [66-67] against *P. aeruginosa* C25 [23]. The formers were performed using 2-fold increasing concentrations of both antibiotic (from 0.125 to 128 µg/ml) and berberine (from 10 to 320 µg/ml). Since berberine was resuspended in 50% DMSO and 50% methanol, the upper limit of the concentrations range tested was determined keeping in mind to respect the recommended final concentration of 1% DMSO as close as we could; a 2-fold decrease of tobramycin MIC was interpreted as synergy[68]. The berberine concentrations resulting in synergism with tobramycin were selected for further assays in association with serial tobramycin concentrations against additional *P. aeruginosa* strains.

Time-kill curve analysis was performed as described by Isenberg [69]. Tobramycin concentrations ranging from 1/2x to 2xMIC were used alone and in combination with the lowest active concentration of berberine resulted from checkerboard assays. *P. aeruginosa* C95 was used as the test strain at a concentration of 10^5 CFU/ml. The dynamic of the bactericidal activity of the combination tobramycin-berberine was evaluated by CFU counts after 2, 4, 6, 8 and 24 hours incubation at 37 °C. Any increase ≥ 1log of the bactericidal power of the association compared to that of the antibiotic alone, was considered as a sign of synergy.

PCR assays. PCR assays were performed using the primer pairs previously described targeting *mexY* [70], *ndvB* [64], *rmtA* [71] and *ant(2")-Ia* [69] and 5 µl of bacterial DNA, extracted as described by Hynes at al.[67] *ndvB* encodes a glucosyltransferase able to sequester the aminoglycosides[64], *rmtA* a 16S rRNA methylase[70] and *ant(2")-Ia* an aminoglycoside-modifying nucleotidyltransferase[71].

P. aeruginosa PAO1 [65], *P. aeruginosa* PA14 [64] and *P. aeruginosa* AR86 were used as positive controls in assays targeting *mexY, ndvB* and *ant(2")-Ia* respectively, whereas *rmtA* amplicons were sequenced and the obtained sequences analyzed for their correspondence with that deposited in Genbank (accession number NG_048057)[72].

Hemolysis assays. Hemolysis assays were performed as described by Chongsiriwatana et al. [73]. Briefly, four ml of freshly drawn, heparanized human blood were diluted with 25 ml of phosphate buffered saline (PBS), pH 7.4. After 3x washing in 25 ml PBS, the pellet was resuspended in PBS to ~ 20 vol%. One-hundred µl of erythrocyte suspension was added to 100 µl of different concentrations of berberine to be tested (1:2 serial dilutions in PBS,). The negative and the positive control were 100 µl of PBS and 100 µl of 0.2 vol% Triton X-100, respectively. Each condition was tested in triplicate. After 1 h incubation at 37°C each well was supplemented with 150 µl of PBS and the plate centrifuged at 1.200 x g for 15 min. The supernatant was diluted in 1:3 and transferred in a new plate and its OD_{540} [74-75] measured using the Synergy HT MicroPlate Reader Spectrophotometer (BioTek, Winooski, VT, USA).

The hemolysis (%) was determined as follows: $[(A - A_0)/(A_{total} - A_0)] \times 100$

where A is the absorbance of the test well, A0 the absorbance of the negative control, and A_{total} the absorbance of the positive control; the mean value of the three replicates was recorded.

ACKNOWLEDGEMENTS

This work was supported by Università Politecnica delle Marche, Progetto Strategico di Ateneo, project "Pseudomonas aeruginosa biofilm persistent infections: improved detection of non-culturable forms and identification of efflux systems inhibitors (EPIs) from natural sources able to counteract biofilm development antibiotic efflux using a combined *in silico/in vitro* screening", 2016-2018 and by the grant from the Italian Cystic Fibrosis Foundation FFC #13/2017.

REFERENCES

1. D. Hocquet, C. Vogne, F. El Garch, A. Vejux, N. Gotoh, A. Lee, O. Lomovskaya and P. Plesiat, MexXY-OprM efflux pump is necessary for a adaptive resistance of *Pseudomonas aeruginosa* to aminoglycosides, *Antimicrob Agents Chemother,* 2003, **47**, 1371-1375.
2. Y. Morita, J. Tomida, Y. Kawamura, MexXY multidrug efflux system of *Pseudomonas aeruginosa*, *Front Microbiol*, 2012, **3,** 408.
3. Y. Morita, J. Tomida, Y. Kawamura, Responses of *Pseudomonas aeruginosa* to antimicrobials, *Front Microbiol,* 2014, **4** 422.
4. S. Fraud, K. Poole, Oxidative stress induction of the MexXY multidrug efflux genes and promotion of aminoglycoside resistance development in *Pseudomonas aeruginosa*, *Antimicrob Agents Chemother*, 2011, **55** 1068-1074.
5. K. Jeannot, M.L. Sobel, F. El Garch, K. Poole, P. Plesiat, Induction of the MexXY efflux pump in *Pseudomonas aeruginosa* is dependent on drug-ribosome interaction, *J Bacteriol*, 2005, **187**, 5341-5346.
6. R.E. Caughlan, S. Sriram, D.M. Daigle, A.L. Woods, J. Buco, R.L. Peterson, J. Dzink-Fox, S. Walker, C.R. Dean, Fmt bypass in *Pseudomonas aeruginosa* causes induction of MexXY efflux pump expression, *Antimicrob Agents Chemother*, 2009, **53**, 5015-5021.
7. C. Muller, P. Plesiat, K. Jeannot, A two-component regulatory system interconnects resistance to polymyxins, aminoglycosides, fluoroquinolones, and beta-lactams in *Pseudomonas aeruginosa*, *Antimicrob Agents Chemother*, 2011, **55,** 1211-1221.
8. N. Hoiby, T. Bjarnsholt, M. Givskov, S. Molin, O. Ciofu, Antibiotic resistance of bacterial biofilms, *Int J Antimicrob Agents*, 2010, **35**, 322-332.
9. M.H. Prickett, A.R. Hauser, S.A. McColley, J. Cullina, E. Potter, C. Powers, M. Jain, Aminoglycoside resistance of *Pseudomonas aeruginosa* in cystic fibrosis results from convergent evolution in the mexZ gene, *Thorax*, 2017, **72** 40-47.

10. S. Islam, H. Oh, S. Jalal, F. Karpati, O. Ciofu, N. Hoiby, B. Wretlind, Chromosomal mechanisms of aminoglycoside resistance in *Pseudomonas aeruginosa* isolates from cystic fibrosis patients, *Clin Microbiol Infect*, 2009, **15**, 60-66.
11. B. Henrichfreise, I. Wiegand, W. Pfister, B. Wiedemann, Resistance mechanisms of multiresistant *Pseudomonas aeruginosa* strains from Germany and correlation with hypermutation, *Antimicrob Agents Chemother*, 2007, **51**, 4062-4070.
12. J.M. Blair, L.J. Piddock, Structure, function and inhibition of RND efflux pumps in Gram-negative bacteria: an update, *Curr Opin Microbio*l, 2009, **12**, 512-519.
13. S. Murakami, R. Nakashima, E. Yamashita, T. Matsumoto, A. Yamaguchi, Crystal structures of a multidrug transporter reveal a functionally rotating mechanism, *Nature*, 2006,**443,** 173-179.
14. M.A. Seeger, A. Schiefner, T. Eicher, F. Verrey, K. Diederichs, K.M. Pos, Structural asymmetry of AcrB trimer suggests a peristaltic pump mechanism, *Scienc*e, 2006, **313**, 1295-1298.
15. C.H. Lau, D. Hughes, K. Poole, MexY-promoted aminoglycoside resistance in *Pseudomonas aeruginosa*: involvement of a putative proximal binding pocket in aminoglycoside recognition, *MBio*, 2014, **5**, e01068.
16. V.K. Ramaswamy, A.V. Vargiu, G. Malloci, J. Dreier, P. Ruggerone, Molecular Determinants of the Promiscuity of MexB and MexY Multidrug Transporters of *Pseudomonas aeruginosa*, *Front Microbiol.* 2018, **9**, 1144 (1-17).
17. S.S. Aghayan, H. Kalalian Mogadam, M. Fazli, D. Darban-Sarokhalil, S.S. Khoramrooz, F. Jabalameli, S. Yaslianifard, M. Mirzaii, The Effects of Berberine and Palmatine on Efflux Pumps Inhibition with Different Gene Patterns in *Pseudomonas aeruginosa* Isolated from Burn Infections, *Avicenna J Med Biotechnol*,2017, **9,** 2-7.
18. M.M. Kheir, Y. Wang, L. Hua, J. Hu, L. Li, F. Lei, L. Du, Acute toxicity of Berberine and its correlation with the blood concentration in mice, *Food Chem Toxicol*, 2010, **48**,1105-1110.
19. Morita Y, Nakashima K, Nishino K, Kotani K, Tomida J, Inoue M, Kawamura Y. Berberine Is a Novel Type Efflux Inhibitor Which Attenuates the MexXY-Mediated Aminoglycoside Resistance in *Pseudomonas aeruginosa*. F*ront Microbio*l. 2016, **7**, 1223.
20. J. Lam, S. Vaughan, M.D. Parkins, Tobramycin Inhalation Powder (TIP): An Efficient Treatment Strategy for the Management of Chronic *Pseudomonas Aeruginosa* Infection in Cystic Fibrosis, *Clin Med Insights Circ Respir Pulm Med*, 2013, **7** , 61-77.
21. G. Mangiaterra, E. Laudadio, M. Cometti, G. Mobbili, C. Minnelli, L. Massaccesi, B. Citterio, F. Biavasco, R. Galeazzi, Inhibitors of multidrug efflux pumps of *Pseudomonas aeruginosa* from natural sources: An *in silico* high-throughput virtual screening and in vitro validation, *Med Chem Res*, 2017, **26**, 414–430.
22. T. Eicher, H.J. Cha, M.A. Seeger, L. Brandstatter, J. El-Delik, J.A. Bohnert, W.V. Kern, F. Verrey, M.G. Grutter, K. Diederichs, K.M. Pos, Transport of drugs by the multidrug transporter AcrB involves an access and a deep binding pocket that are separated by a switch-loop, *Proc Natl Acad Sci U S* A, 2012, **109,** 5687-5692.
23. R. Nakashima, K. Sakurai, S. Yamasaki, K. Nishino, A. Yamaguchi, Structures of the multidrug exporter AcrB reveal a proximal multisite drug-binding pocket, *Nature*, 2011, **480,** 565-569.
24. A.V. Vargiu, H. Nikaido, Multidrug binding properties of the AcrB efflux pump characterized by molecular dynamics simulations, *Proc Natl Acad Sci U S A*, 2012, **109,** 20637-20642.
25. F. Husain, H. Nikaido, Substrate path in the AcrB multidrug efflux pump of Escherichia coli, *Mol Microbiol*, 2010, **78** , 320-330.
26. X.Q. Yao, N. Kimura, S. Murakami, S. Takada, Drug uptake pathways of multidrug transporter AcrB studied by molecular simulations and site-directed mutagenesis experiments, *J Am Chem Soc*, 2013,**135,** 7474-7485.
27. E.W. Yu, J.R. Aires, G. McDermott, H. Nikaido, A periplasmic drug-binding site of the AcrB multidrug efflux pump: a crystallographic and site-directed mutagenesis study, *J Bacteriol*, 2005, **187,** 6804-6815.
28. D. Fedeli, M. Montani, L. Bordoni, R. Galeazzi, C. Nasuti, L. Correia-Sa, V.F. Domingues, M. Jayant, V. Brahmachari, L. Massaccesi, E. Laudadio, R. Gabbianelli, *In vivo* and *in silico* studies to identify mechanisms associated with Nurr1 modulation following early life exposure to permethrin in rats, *Neuroscience*, 2017, **340**, 411-423.

29. R. Galeazzi, L. Massaccesi, F. Piva, G. Principato, E. Laudadio, Insights into the influence of 5-HT2c aminoacidic variants with the inhibitory action of serotonin inverse agonists and antagonists, *J Mol Model*, 2014, **20** 2120.
30. E.Laudadio, G. Mobbili, C. Minnelli, L.Massaccesi, R. Galeazzi, Salts influence cathechins and flavonoids encapsulation in liposomes: a molecular dynamics investigation, *Molecular informatics*, 2017**, 36** (11), 1700059.
31. M. Baldassarre, R.Galeazzi, B. Maggiore, F.Tanfani, A. Scirè, Bovine α1-acid glycoprotein, a thermostable version of its human counterpart: Insights from Fourier transform infrared spectroscopy and in silico modeling, *Biochimie*, 2014, **102**, 19-28.
32. R. Galeazzi, P. Bruni, E. Crucianelli, E. Laudadio, M. Marini, L. Massaccesi, G. Mobbili, M. Pisani, Liposome-based gene delivery systems containing a steroid derivative: computational and small angle X-ray diffraction study, *RSC Advances*, 2015, **5**, 54070-54078.
33. M.J. Abraham, T. Murtola, R. Schulz, S.Páll, J. C.Smith, B. Hess, E. Lindahl, GROMACS: High performance molecular simulations through multi-level parallelism from laptops to supercomputers, Software X, 2015, 1-2, 19-25.
34. T.H. Ogunwa,E. Laudadio,R. Galeazzi, T. Miyanishi, *Pharmaceuticals (Basel)*, 2019, **12**(2), E58. doi: 10.3390/ph12020058.
35. A. Spitaleri,S. Decherchi, A. Cavalli,W. Rocchia, Fast Dynamic Docking Guided by Adaptive Electrostatic Bias: The MD-Binding Approach, *J Chem Theory Comput*. 2018, **14**(3), 1727-1736.
36. A. Yamaguchi, R. Nakashima, K. Sakurai, Structural basis of RNDtype multidrug exporters. *Front. Microbiol.* 2015, **6**, 327.
37. L. Marsh, Strong ligand-protein interactions derived from diffuse ligand interactions with loose binding sites. *Biomed Res. Int.* 2015, 746980. doi: 10.1155/2015/746980
38. T.F. Mah, B. Pitts, B. Pellock, G.C. Walker, P.S. Stewart, G.A. O'.Toole, A genetic basis for Pseudomonas aeruginosa biofilm antibiotic resistance, *Nature*, 2003, **426**, 306-310.
39. M100 Performance Standards for Antimicrobial Susceptibility Testing, in, Clinical and Laboratory Standards Institute (CLSI) Wayne, Pennsylvania, USA, 2017.
40. Zohra M, Fawzia A. Hemolytic activity of different herbal extracts used in Algeria, *Int J Pharm Sci Res*, 2014, **5**, 8495.
41. Y. Zhang, I-TASSER server for protein 3D structure prediction, *BMC Bioinformatics*, 9 (2008) 40.
42. A. Roy, A. Kucukural, Y. Zhang, I-TASSER: a unified platform for automated protein structure and function prediction, *Nat Protoc*, 2010, **5**, 725-738.
43. S. Bienert, A. Waterhouse, T.A. de Beer, G. Tauriello, G. Studer, L. Bordoli, T. Schwede, The SWISS-MODEL Repository-new features and functionality, *Nucleic Acids Res*, 2017, **45**, D313-D319.
44. J.P. Rodrigues, M. Levitt, G. Chopra, KoBaMIN: a knowledge-based minimization web server for protein structure refinement, *Nucleic Acids Res*, 2012, **40**, W323-328.
45. M.W.M. R.A. Laskowski, D.S. Moss, J. M. Thornton, PROCHECK: a program to check the stereochemical quality of protein structures, *Journal of Applied Crystallography*, 1993, **26**, 283-291.
46. E.F. Pettersen, T.D. Goddard, C.C. Huang, G.S. Couch, D.M. Greenblatt, E.C. Meng, T.E. Ferrin, UCSF Chimera--a visualization system for exploratory research and analysis, *J Comput Chem*, 2004, **25,** 1605-1612.
47. R.Gabbianelli, M. Carloni, F. Marmocchi, C. Nasuti, D. Fedeli, E. Laudadio, L. Massaccesi, R.Galeazzi, Permethrin and its metabolites affect Cu/Zn superoxide conformation: fluorescence and in silico evidences, *Mol Biosyst*, 2015, **11,** 208-217.
48. R. Galeazzi, E. Laudadio,E. Falconi, L. Massaccesi,L. Ercolani, G. Mobbili, C. Minnelli, A. Scirè,L. Cianfruglia, T. Armeni, Protein-protein interactions of human glyoxalase II: findings of a reliable docking protocol, *Org Biomol Chem*. 2018, 16(28):5167-5177.
49. R. Galeazzi, G. Martelli, E. Marcucci, M. Orena, S. Rinaldi, R. Lattanzi, L. Negri, Analogues of both Leu- and Met-enkephalin containing a constrained dipeptide isostere prepared from a Baylis-Hillman adduct, *Amino Acids*, 2010, **38**, 1057-1065.
50. J.C. Gordon, J.B. Myers, T. Folta, V. Shoja, L.S. Heath, A. Onufriev, H++: a server for estimating pKas and adding missing hydrogens to macromolecules, *Nucleic Acids Res*, 2005, **33,** W368-371.
51. O. Trott, A.J. Olson, AutoDock Vina: improving the speed and accuracy of docking with a new scoring function, efficient optimization, and multithreading, *J Comput Chem*, 2010, **31** , 455-461.

52. M.W. Chang, C. Ayeni, S. Breuer, B.E. Torbett, Virtual screening for HIV protease inhibitors: a comparison of AutoDock 4 and Vina, *PLoS One*, 2010, **5**, e11955.
53. A. Lavecchia, C. Di Giovanni, Virtual screening strategies in drug discovery: a critical review, *Curr Med Chem*, 2013, **20,** 2839-2860.
54. E. Glaab, Building a virtual ligand screening pipeline using free software: a survey, *Brief Bioinform*, 2016 **17**, 352-366.
55. G.M. Morris, R. Huey, W. Lindstrom, M.F. Sanner, R.K. Belew, D.S. Goodsell, A.J. Olson, AutoDock4 and AutoDockTools4: Automated docking with selective receptor flexibility, *J Comput Chem*, 2009,**30,** 2785-2791.
56. A.T. Guy, T.J. Piggot, S. Khalid, Single-stranded DNA within nanopores: conformational dynamics and implications for sequencing; a molecular dynamics simulation study, *Biophys J*, 2012,**103,** 1028-1036.
57. C.J. William L. Jorgensen, Temperature dependence of TIP3P, SPC, and TIP4P water from NPT Monte Carlo simulations: Seeking temperatures of maximum density , *J Comput Chem*, 1998, **19,** 8.
58. X. Hu, J. Xie, S. Hu, L. Zhang, Y. Dong, Exploration of the binding affinities between ecdysone agonists and EcR/USP by docking and MM-PB/GBSA approaches, *J Mol Model*, 2017,**23** , 166.
59. Z. Dolatkhah, S. Javanshir, A.S. Sadr, J. Hosseini, S. Sardari, Synthesis, Molecular Docking, Molecular Dynamics Studies, and Biological Evaluation of 4H-Chromone-1,2,3,4-tetrahydropyrimidine-5-carboxylate Derivatives as Potential Antileukemic Agents, *J Chem Inf Model*, 2017, **57**, 1246-1257.
60. T. Venken, D. Krnavek, J. Munch, F. Kirchhoff, P. Henklein, M. De Maeyer, A. Voet, An optimized MM/PBSA virtual screening approach applied to an HIV-1 gp41 fusion peptide inhibitor, *Proteins*, 2011, **79**, 3221-3235.
61. U.P. Essmann, Lalith; Berkowitz, Max L.; Darden, Tom; Lee, Hsing; Pedersen, Lee G., A smooth particle mesh Ewald method, *J Chem Phys*, **103** ,1995, 16.
62. R. Kumari, R. Kumar, A. Lynn, g_mmpbsa--a GROMACS tool for high-throughput MM-PBSA calculations, *J Chem Inf Model*, 2014, **54,** 1951-1962.
63. R. Bhattacharjee, A. Devi, S. Mishra, Molecular docking and molecular dynamics studies reveal structural basis of inhibition and selectivity of inhibitors EGCG and OSU-03012 toward glucose regulated protein-78 (GRP78) overexpressed in glioblastoma, *J Mol Model*, 2015, **21,** 272.
64. *T. Beaudoin, L. Zhang, A.J. Hinz, C.J. Parr, T.F. Mah, The biofilm-specific antibiotic resistance gene ndvB* is important for expression of ethanol oxidation genes in *Pseudomonas aeruginosa* biofilms, *J Bacteriol*, 2012, **194,** 3128-3136.
65. H.A. Terzi, C. Kulah, I.H. Ciftci, The effects of active efflux pumps on antibiotic resistance in Pseudomonas aeruginosa, World, *J Microbiol Biotechnol*, 2014, **30,** 2681-2687.
66. M07-A10: Methods for Dilution Antimicrobial Susceptibility Tests for Bacteria That Grow Aerobically; Approved Standard-Tenth Edition, in, Clinical and Laboratory Standards Institute (CLSI), 2017.
67. H.D. Isenberg, Clinical Microbiology Procedures Handbook ASM, Washington DC, 1992.
68. RP. Lamers, JF. Cavallari, LL. Burrows. The efflux inhibitor phenylalanine-arginine beta-naphthylamide (PAβN) permeabilizes the outer membrane of gram-negative bacteria, *PLoS On*e, 2013, **8**, e60666.
69. A.D. Michalska, P.T. Sacha, D. Ojdana, A. Wieczorek, E. Tryniszewska, Prevalence of resistance to aminoglycosides and fluoroquinolones among *Pseudomonas aeruginosa* strains in a University Hospital in Northeastern Poland, *Braz J Microbiol*, 2014,**45,** 1455-1458.
70. H. Oh, J. Stenhoff, S. Jalal, B. Wretlind, Role of efflux pumps and mutations in genes for topoisomerases II and IV in fluoroquinolone-resistant *Pseudomonas aeruginosa* strains, *Microb Drug Resist*, 2003, **9,** 323-328.
71. K. Yamane, Y. Doi, K. Yokoyama, T. Yagi, H. Kurokawa, N. Shibata, K. Shibayama, H. Kato, Y. Arakawa, Genetic environments of the rmtA gene in *Pseudomonas aeruginosa* clinical isolates, *Antimicrob Agents Chemother*, 2004, **48,** 2069-2074.
72. W.L. Hynes, J.J. Ferretti, M.S. Gilmore, R.A. Segarra, PCR amplification of streptococcal DNA using crude cell lysates, *FEMS Microbiol Let*t, 1992, **73**, 139-142
73. Chongsiriwatana NP, Patch JA, Czyzewski AM, Dohm MT, Ivankin A, Gidalevitz D, Zuckermann RN, Barron AE Peptoids that mimic the structure, function and mechanism of helical antimicrobial peptides, P*roc Natl Acad Sci U.S.A.*, 2008, **105**,2794–2799.
74. W.L. Hynes, J.J. Ferretti, M.S. Gilmore, R.A. Segarra, PCR amplification of streptococcal DNA using crude cell lysates, *FEMS Microbiol Let*t, 1992, **73**, 139-142.

75. Zohra M, Fawzia A. Hemolytic activity of different herbal extracts used in Algeria, *Int J Pharm Sci Res*, 2014, **5**, 8495.